Complexity of vesicle microcirculation

B. Kaoui,[1] N. Tahiri,[2,3] T. Biben,[4] H. Ez-Zahraouy,[3] A. Benyoussef,[3] G. Biros,[5] and C. Misbah[2]

[1]*Technische Universiteit Eindhoven, Postbus 513, 5600 MB Eindhoven, The Netherlands*

[2]*Laboratoire Interdisciplinaire de Physique, University of Grenoble, 1/CNRS, UMR5588, 140 Avenue de la Physique, Grenoble F-38041, France*

[3]*Laboratoire de Magnétisme et de la Physique des Hautes Energies, Faculté des Sciences, Université Mohammed V, Avenue Ibn Battouta, Rabat B.P. 1014, Morocco*

[4]*Laboratoire PMCN, Université de Lyon, CNRS, UMR 5586, F-69622 Villeurbanne Cedex, France*

[5]*Georgia Institute of Technology, 1324 Klaus Advanced Computing Building, 266 Ferst Drive, Atlanta, Georgia 30332-0765, USA*

(Received 28 March 2011; revised manuscript received 5 September 2011; published 5 October 2011)

This study focuses numerically on dynamics in two dimensions of vesicles in microcirculation. The method used is based on boundary integral formulation. This study is inspired by the behavior of red blood cells (RBCs) in the microvasculature. Red RBCs carry oxygen from the lungs and deliver it through the microvasculature. The shape adopted by RBCs can affect blood flow and influence oxygen delivery. Our simulation using vesicles (a simple model for RBC) reveals unexpected complexity as compared to the case where a purely unbounded Poiseuille flow is considered [Kaoui, Biros, and Misbah, Phys. Rev. Lett. **103**, 188101 (2009)]. In sufficiently large channels (in the range of 100 μm; the vesicle size and its reduced volume are taken in the range of those of a human RBC), such as arterioles, a slipperlike (asymmetric) shape prevails. A parachutelike (symmetric) shape is adopted in smaller channels (in the range of 20 μm, as in venules), but this shape loses stability and again changes to a pronounced slipperlike morphology in channels having a size typical of capillaries (5–10 μm). Stiff membranes, mimicking malaria infection, for example, adopt a centered or off-centered snakelike locomotion instead (the denomination *snaking* is used for this regime). A general scenario of how and why vesicles adopt their morphologies and dynamics among several distinct possibilities is provided. This finding potentially points to nontrivial RBCs dynamics in the microvasculature.

DOI: 10.1103/PhysRevE.84.041906 PACS number(s): 87.16.D−, 83.50.Ha, 83.80.Lz

I. INTRODUCTION

The present study, which will be performed on a model system (namely, vesicles in two dimensions), is inspired by some intriguing behaviors encountered in the red blood cells (RBCs) microcirculation. For this purpose it seems worthwhile to recall some of the main properties of blood and the results achieved on single RBCs in microcirculation. RBCs occupy approximately 45% of the total blood volume, whereas other blood corpuscles including white cells compose less than 1%. The remaining blood volume consists of plasma. RBCs' main function is to transport oxygen from the lungs to bodily tissues via the microcirculatory system (the arterioles and capillaries). Early in the 19th century, direct measurements of arterial and venous blood pressures by Poiseuille [1,2] revealed that microcirculation causes most of the viscous resistance to blood flow. This resistance depends both on the architecture of the microvascular network and on the rheological behavior of blood flowing through it, which in turn is governed by the shape of the RBCs. An understanding of the morphology of RBCs and their dynamics in the microvasculature is essential to understanding blood flow.

A long-standing puzzle is why do RBCs adopt an asymmetric shape (called a slipper) in microcirculation, despite a symmetric flow. In vivo the volume fraction of RBCs in the microvasculature (also called hematocrit) is about 20% (unlike in macrocirculation where the hematocrit is about 45%), so that RBCs are in a close contact with each other. The first comprehensive experimental report on the slipper phenomenon is that of Skalak and Branemark [3] (who studied a cluster of cells), followed by another experimental study by Gaehtgens *et al*. [4]. Subsequent studies on single RBCs exhibiting a slipper shape in a glass tube were briefly reported by Secomb *et al*. [5] and analyzed in more detail by Guido and Tomaiuolo [6]. This problem was revisited more recently [7,8].

A first theory, using a lubrication approximation, was proposed by Secomb and Skalak [9], and the slipper shape was later observed in numerical simulations by Pozrikidis [10]. Two-dimensional (2D) simulations were considered more recently by Secomb *et al*. [5], who reported on the slipper shape. Recently, considering [11] an unbounded parabolic velocity profile, the slipper shape was shown to be an intrinsic configuration resulting from the instability of the symmetric (parachute) shape. However, in this paper we show that accounting for the walls leads to an unexpected complexity, as we shall see. Five distinct morphologies and dynamics are identified, depending on flow and structural parameters.

This paper is organized as follows. In Sec. II we describe the model used to solve this problem. In Sec. III we present the main results. Section IV is devoted to some concluding remarks.

II. MODEL

We consider a vesicle, a closed membrane made of a bilayer of phospholipid, which is a simplistic representation of a RBC.

This simplification is essential in order to identify the basic ingredients in a progressive manner.

We consider a plane Poiseuille flow along the x direction [we have also explored partially the three-dimensional (3D) case] given by

$$v_{0x} = v_{\max}\left[1 - \frac{y^2}{(w/2)^2}\right], \tag{1}$$

where w is the channel width and the delimiting boundaries are located at $y = \pm w/2$, so that $v_{0x}(y = \pm w/2) = 0$, and $v_{\max}$ is the maximum velocity. The shear rate at the wall is given by $\dot{\gamma}_w = 4v_{\max}/w$. The walls are advected along the x axis with the vesicle center of mass (the so-called camera method). The lateral extension of the wall (i.e., in the x direction) is taken very large as compared to the vesicle size (at least 100 times bigger) so that on the lateral sides the flow is practically unperturbed. The vesicle membrane acts on the fluid via bending forces, while the local membrane area remains unstretched; the membrane develops tension forces ζ that prevent extension (or compression). Both effects lead to the following membrane force per unit area [12]:

$$\mathbf{f} = \kappa\left[\frac{d^2c}{ds^2} + \frac{1}{2}c^3\right]\mathbf{n} - \zeta c\mathbf{n} + \frac{d\zeta}{ds}\mathbf{t}. \tag{2}$$

Here c is the membrane curvature, $\mathbf{n}$ and $\mathbf{t}$ are the unit normal and tangent vectors, s is the arclength coordinate, and κ is the membrane bending rigidity. Blood vessels are endowed with elasticity reacting to stresses from the fluid. In the microvasculature (especially in the capillaries) the inertia is small and the Stokes regime is a good approximation. We have extended the method used in Ref. [13] in order to include a second wall, and several tests have also been made by using the code described in Ref. [14]. The vesicle membrane and the vessel wall forces modify the imposed Poiseuille flow so that the velocity of each point of the membrane takes the following form (the boundary integral formulation):

$$\mathbf{v}(\mathbf{x}_0) = \mathbf{v}_{0x} + \frac{1}{\eta}\oint_{\text{vesicle}} \mathbf{G}(\mathbf{x} - \mathbf{x}_0)\cdot\mathbf{f}(\mathbf{x})ds + \frac{1}{\eta}\int_{\text{walls}} \mathbf{G}(\mathbf{x} - \mathbf{x}_0)ds\cdot\mathbf{f}_w(\mathbf{x}), \tag{3}$$

where η is the fluid viscosity, and

$$G_{ij}(\mathbf{x} - \mathbf{x}_0) = -\delta_{ij}\ln|\mathbf{x} - \mathbf{x}_0| + \frac{(\mathbf{x} - \mathbf{x}_0)_i(\mathbf{x} - \mathbf{x}_0)_j}{|\mathbf{x} - \mathbf{x}_0|^2}.$$

The first integral in Eq. (3) is performed on the vesicle boundary and the second one on the delimiting boundaries located at $y = \pm w/2$. We consider flexible walls having a reaction force per unit area given by $\mathbf{f}_w$. For simplicity we consider that the wall displacement is proportional to the deflexion from the straight equilibrium $\mathbf{u}$, so that $\mathbf{f}_w = -K\mathbf{u}$, where K is an elastic constant (having a dimension of a force per unit volume). Equation (3) is solved numerically (as described in Refs. [13] and [14]).

Our results are summarized in terms of dimensionless parameters:

$$C_\kappa = \eta\dot{\gamma}_w R^3/\kappa,$$

expressing the flow strength over the vesicle deformation,

$$C_w = \eta\dot{\gamma}_w/KR,$$

expressing the flow strength over the blood vessel wall deformation, and

$$C_n = \frac{2R}{W},$$

which is the degree of confinement (vesicle diameter—the diameter of a sphere having the same area, $2R$—over that of the blood vessel). We have fixed the vesicle reduced area (its actual area over that of a circle having the same perimeter) to a value close to that provided in the literature for human RBC, namely 0.6.

The sites in the microvasculature where oxygen delivery occurs are arterioles [15] (with diameters of approximately 50 μm) and capillaries (with diameters from 5 to 10 μm); the corresponding average wall shear rates are about 8000 and 1000/s, respectively. Membrane rigidity for a healthy membrane is [16] $\kappa \simeq 3\times 10^{-19}J$, and the typical RBC diameter (the diameter of a sphere having the same area) is about 6 μm. Finally, the plasma viscosity is $\eta \simeq 10^{-3}$ P. Using these values, we found a range of $C_\kappa = 20$ to 100. Greater membrane rigidity, as observed in infected cells [17] (the rigidity of which may be one order of magnitude greater), yields smaller values for C_κ, with $C_\kappa \simeq 1$ to 10. We thus explored the range $C_\kappa = 1$ to 100, which covers a wide interval of relevant values for healthy and unhealthy cells. The degrees of confinement of arterioles and capillaries are approximately 0.15 and 0.8, respectively. We explored the range of $C_n = 0.1$ to 0.8 in our simulations.

The vessel wall elasticity is basically due to the glycocalyx [18] (a soft, brushlike biopolymer covering the endothelium, on which cells perform "surfing"). The wall rigidity is estimated to be [13] $K \sim E/W$ where $E \sim 10Pa$ [18] is the effective Young modulus and $W \sim 0.2$ μm [18] is the glycocalyx thickness. We thus obtain typically $C_w \simeq 0.1$. This value is small compared to C_κ. In other words, the wall is stiff compared to the membrane, so its response to fluid stresses is quasi-instantaneous.

We have first used in our simulation $C_w = 0.01$ and then increased it by a factor of about 5 without any significant changes of the results presented below (as we shall see below). The same holds for the rigid wall (by using the code developed in Ref. [14]).

III. RESULTS AND DISCUSSION

We first set $C_\kappa = 10$ (a typical value in the microvasculature) and increased the degree of confinement. At a small degree of confinement equal to 0.1, a given initial shape converges to a slipper, with the parachute being unstable. The results of this weakly confined simulation agree with our recent study [11] that considered completely unbounded flow. By increasing the confinement, we discovered that the slipper disappears in the range of $0.3 < C_\kappa < 0.6$. That is, the slipper becomes unstable, whereas a symmetric parachute regains stability. An interesting fact is that a further increase in confinement beyond 0.6 results in the parachute becoming unstable in favor of a pronounced slipper that is reminiscent (right in Fig. 1) of RBC shapes observed experimentally [3]. Interestingly, the slipper occurs in weakly and strongly confined sites of the microvasculature where oxygen supply

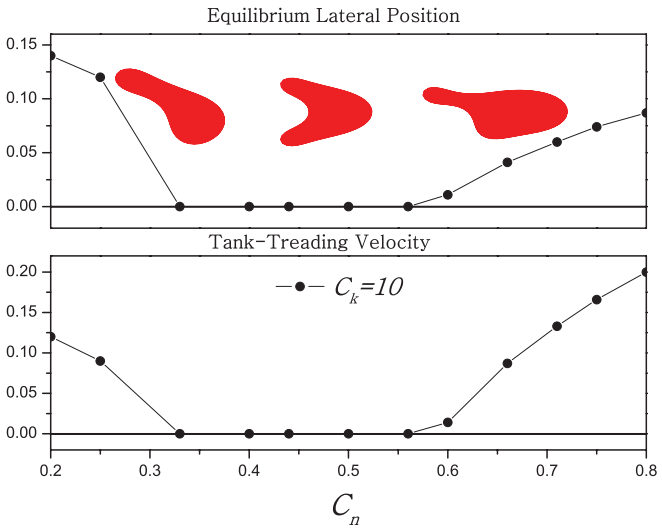

FIG. 1. (Color online) The center of mass (top) of the vesicle and the tank-treading velocity (bottom), as a function of confinement, and illustrative shapes obtained numerically. A slipper has a nonzero center of mass and tank-treading velocity, unlike the parachute shape where both are zero. The symbols refer to the computed data, while the line is a guide for the eye.

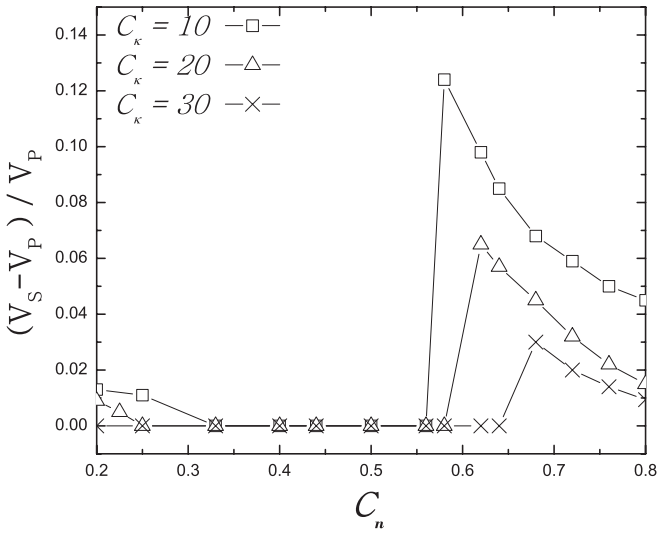

FIG. 2. The flow efficiency of the slipper shape compared to that of parachute-shaped cells as a function of confinement for different values of C_κ. The symbols refer to the computed data, while the line is a guide for the eye.

takes place (arterioles and capillaries). The stable slipper solution obtained for weak confinement (left in Fig. 1) is a distinct solution from that obtained for strong confinement (right in Fig. 1). We use the abbreviations U-Sl and C-Sl for unconfined and confined slippers, respectively. Figure 1 (upper panel) shows the position of the center of mass of the vesicle as a function of confinement and corresponding shapes.

The instability of a symmetric shape in favor of a slipper is found to be a robust feature, which gives an unambiguous reason for its prevailing in arterioles and capillaries. However, it would be interesting to determine whether there is some basic, intuitive reason for the prevailing slipper shape. For this purpose, we first addressed the question of flow efficiency. To quantify it, we compared the speed of parachute-shaped cells in the unstable domain of the parachute (while unstable, the parachute has a finite lifetime during which its speed can be computed) to that of the slipper shape for the same flow and confinement conditions. Figure 2 shows that the slipper shape always moves faster than the parachute. The gain in flow efficiency reaches as high as 15% (in capillaries) for the range of parameters explored. Another essential feature associated with the slipper is membrane tank treading, which does not occur with symmetric shapes. Figure 1 (lower panel) shows the tank-treading velocity as a function of confinement. Tank-treading entails flow recirculation inside the cell. As the main function of RBCs is oxygen delivery in the microvasculature, the prevalence of the slipper ensures the mixing of hemoglobin as well as of other species inside the cytoplasm, such as Adenosine triphosphate (ATP).

The oxygen diffusion coefficient is of the order of [19] 10^{-5} cm^2/s, meaning that it takes about 0.03 s for oxygen to diffuse inside the RBC, a time during which a RBC would have traveled a distance of about 30 times its radius. ATP diffusion is about 10 times slower than oxygen, implying that its diffusion within a RBC requires about a second, a time during which a RBC travels about 1000 times its radius (the traveled distance is about 0.5 cm). Mixing of the cytoplasm solution constitutes a favorable terrain for chemical release by RBCs. We found that mixing due to tank treading in capillaries occurs in a time of about 0.01 s and is thus significantly faster than oxygen and ATP diffusion. Furthermore, the slipper shape is found to be accompanied by an increase of the wall shear stress. Since stress is linked with ATP release [20] the occurrence of C-Sl cells in the microvasculature may contribute to mechanochemical signaling.

Several diseases, such as malaria, are accompanied by a significant increase in the mechanical modulus of the cell [17]. We examined the effect of increasing the bending rigidity. An increase in bending rigidity (under the same flow conditions) is equivalent to a decrease in C_κ. We thus fixed C_κ to low values, $C_\kappa < 10$. Stiff vesicles in capillaries do not adopt a slipper but rather a shape that exhibits temporal oscillations (this corresponds to a Hopf bifurcation). A snapshot of the motion is shown in Fig. 3. It is reminiscent of snakelike locomotion, so the term *snaking* was adopted for this case. Figure 4 shows the behavior of the center of the vesicle as a function of time in the snaking regime. We show the result for two values of the wall rigidity without any significant change.

In fact, the snaking may either be centered (where the mean value of the center of mass Y_G over a period of oscillation is zero) or off-centered (where the mean value of $Y_G \neq 0$). The observation of each snaking type depends on the flow and structure parameters, as described below. Our results suggest that three important implications in the snaking regime may be expected in microcirculation: (i) in stiff cells, deformation is significantly reduced, presenting a severe obstacle to the squeezing of RBCs through capillaries; (ii) snaking allows for a more efficient flow as compared with the steady bullet shape; and (iii) the tank-treading velocity, however, is significantly smaller as compared to a healthy cell, entailing less efficient mixing of the cell's internal fluid. It was

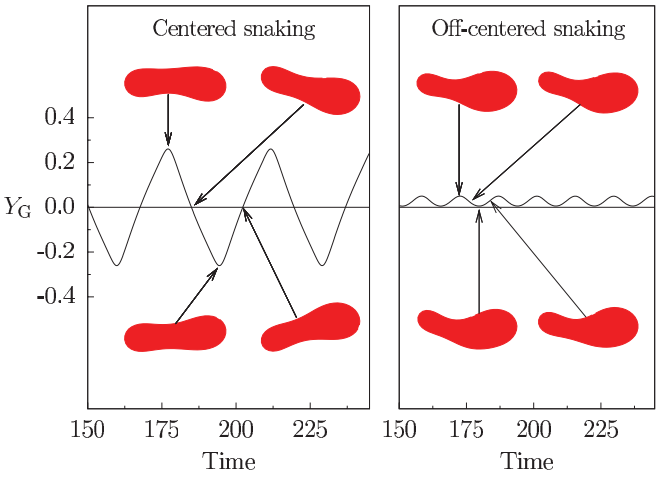

FIG. 3. (Color online) Centered and off-centered snaking motion. The sinlike curves show the center-of-mass position as a function of time. The arrows show the time at which the shape is shown.

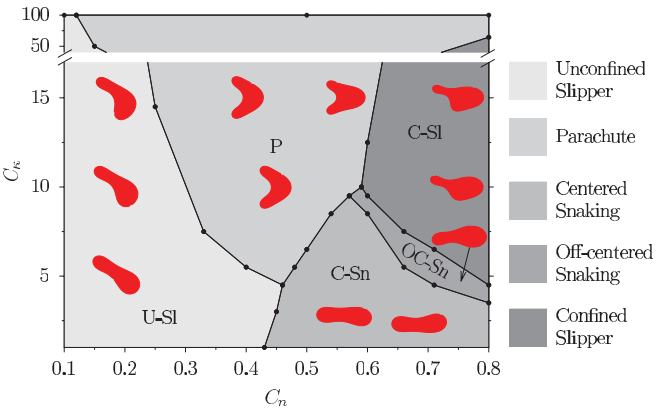

FIG. 5. (Color online) A phase diagram showing five distinct regions depending on flow and structural parameters (represented by the dimensionless number measuring the flow strength over the cell deformation) and the degree of confinement (represented by the vesicle diameter over the channel width). The symbols refer to the computed data, while the line is a guide for the eye.

previously reported [22] that upon an increase of rigidity a vesicle transits from a disklike shape to a prolate one with the main axis directed along the flow direction. This might bear at first sight a similarity with the C-Sn motion, where the main axis is also, on the average, along the flow direction. However, the C-Sn motion is of a flagella type (snacking) resulting from a Hopf bifurcation (this is not to be confused with the elongated shape found in [22], which corresponds to a steady solution).

We performed a systematic analysis in parameter space in order to determine the regions corresponding to each shape and dynamics (Fig. 5). Five distinct regions are revealed (movies of the five shapes and dynamics can be found in [21]). Normal cells (sufficiently large C_κ) in capillaries would correspond to the upper part of the violet region, whereas stiff cells may either correspond to an elongated slipper shape (the bottom of the violet region) or centered and off-centered snaking behavior

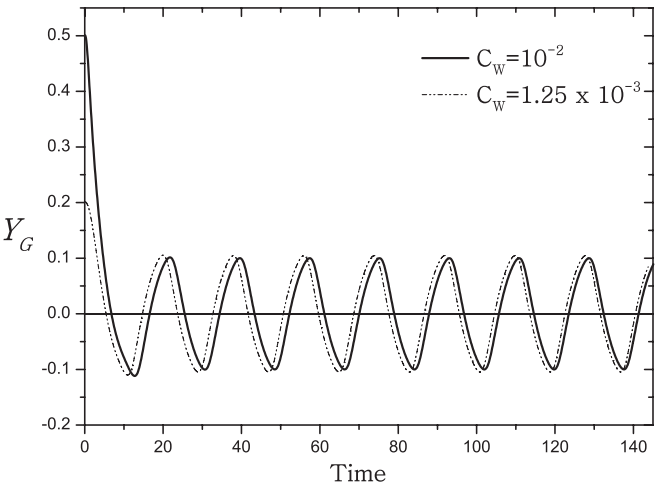

FIG. 4. The evolution of the center of mass of the vesicle as a function of time in the snaking regime. Shown also is the influence of the wall rigidity. We see that an increase of the wall rigidity by a factor of 8 has only a minor effect on the amplitude of oscillation. At initial time the vesicle shows a transient, before exhibiting permanent snaking.

(the light and dark gray regions), depending on the degree of stiffness (the lower part of the diagram corresponds to high stiffness). Available in vitro experimental data [7] are, to some extent, consistent with the present finding regarding the upper part of the phase diagram of Fig. 5. We are not aware of any experimental report on the lower part of Fig. 5 (especially the lower half green domain and the two gray domains). Some experiments on vesicles in a microchannel have been performed [23,24]. In the study by Vitkova *et al.* [23] the explored parameters are $C_\kappa \simeq 1000$ and $C_n \simeq 0.4$–0.6, and only a parachute shape was observed. We have checked that with these values the shape is indeed of a parachute type. Smaller values of C_κ (in the range of 10 to 100) are expected to lead to a slipper shape. We hope that this work will trigger experiments on this model system in order to guide further theoretical development.

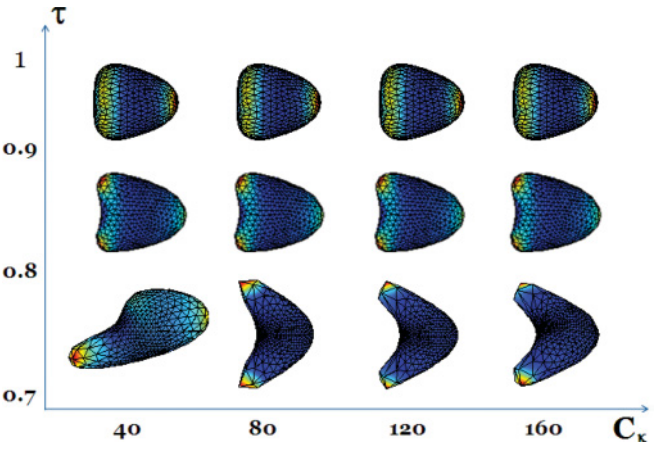

FIG. 6. (Color online) Phase diagram in three dimensions showing the parachute and slipper regimes as a function of the reduced volume τ and the capillary number C_κ. This figure is to be compared with Fig. 2 of Ref. [11] obtained in two dimensions.

IV. CONCLUSION

Our study has focused on 2D dynamics of vesicles. In two dimensions, the notion of shear elasticity looses its meaning, and therefore the vesicle model is a realistic model to represent RBCs. Our recent analysis of 3D vesicles in a simple shear flow [28] has revealed that a quantitative study is too time consuming, so that a systematic analysis of vesicles in three dimensions in a Poiseuille flow remains a formidable task (due to numerical instabilities and the computation time caused by the membrane incompressibility condition, a condition that is not encountered in a simulation of capsules, which are commonly used as candidates for RBCs analysis). Nevertheless, we have attempted to explore the 3D regime in some simple case, namely the unbounded regime explored in two dimensions in [11], in order to analyze the slipper regime. This study should be regarded as very preliminary, and its aim is only to check the possibility of the existence of a slipper shape in the sense discussed in two dimensions in [11]. The numerical method in three dimensions has been discussed in detail in [28].

In Fig. 6 we show the results of the phase diagram obtained in the plane of the following parameters: reduced volume and flow strength (or more precisely the capillary number). This result can be compared with its 2D analog reported in [11]. We see a quite close similarity between the 2D and 3D diagrams, pointing to the fact that the 2D analysis is rather legitimate. This remark is also corroborated by the recent analytical work performed in three dimensions [29], where it is shown that in a plane Poiseuille flow, the picture obtained in two dimensions is captured in three dimensions.

An extension of the present study should incorporate shear elasticity due to the cytoskeleton (a protein network underneath the membrane). RBCs in flow have revealed several dynamic properties that are shared [22,25–27] with vesicles. These observations support the hypothesis that the phospholipid membrane (vesicles) studied here should already capture some essential features. Still, our model remains simplistic and it should be enriched with shear elasticity in the future. We hope that this work will incite experiments also on vesicles and capsules; both are intensively studied as biomimetic models of RBCs.

ACKNOWLEDGMENTS

C. Misbah acknowledges financial support from Centre National d'Études Spatiales and Agence Nationale de la recherche (ANR) "MOSICOB." G. Biros was partially supported by the US National Foundation Award Nos. OCI-1047980 and OCI-0923710.

[1] J. L. M. Poiseuille, D.Sc. thesis, Ecole Polytechnique Paris, 1828.
[2] J. L. M. Poiseuille, J. Physiol. Exp. Pathol. **10**, 277 (1830).
[3] R. Skalak and P. I. Branemark,Science **164**, 717 (1969).
[4] P. Gaehtgens, C. Duhrssen, and K. H. Albrecht, Blood Cells **6**, 799 (1980).
[5] T. W. Secomb, B. Styp-Rekowska, and A. Pries, Ann. Biomed. Eng. **35**, 755 (2007).
[6] S. Guido and G. Tomaiuolo, Soft Matter **5**, 3736 (2009).
[7] M. Abkarian, M. Faivre, R. Horton, K. Smistrup, C. A. Best-Popescu, and H. A. Stone, Biomed. Mater. **3**, 034011 (2008).
[8] S. Guido and G. Tomaiuolo, C. R. Physique **10**, 751 (2009).
[9] T. W. Secomb and R. Skalak, Microvas. Res. **24**, 194 (1982).
[10] C. Pozrikidis, Phys. Fluids **17**, 031503 (2005).
[11] B. Kaoui, G. Biros, and C. Misbah, Phys. Rev. Lett. **103**, 188101 (2009).
[12] B. Kaoui, G. H. Ristow, I. Cantat, C. Misbah, and W. Zimmermann, Phys. Rev. E **77**, 021903 (2008).
[13] J. Beaucourt, T. Biben, and C. Misbah, Europhys. Lett. **67**, 676 (2004).
[14] S. K. Veerapaneni, D. Gueyffier, D. Zorin, and G. Biros, J. Comput. Phys. **228**, 2334 (2009).
[15] Y. C. Fung, *Biomechanics* (Springer, New York, 1990).
[16] T. Betz, M. Lenz, J. F. Joanny, and C. Sykes, Proc. Natl. Acad. Sci. USA **106**, 15320 (2009).
[17] S. Suresh, J. Mater. Res. **21**, 1871 (2006).
[18] S. Weinbaum, J. M. R. Tarbell, and E. R. Damiano, Annu. Rev. Biomed. Eng. **9**, 121 (2007).
[19] J. B. D. Macdougall and M. Mccabe, Nature (London) **215**, 1173 (1967).
[20] J. Wan, W. D. Ristenpart, and H. A. Stone, Proc. Natl. Acad. Sci. USA **105**, 16432 (2008).
[21] See Supplemental Material at http://link.aps.org/supplemental/10.1103/PhysRevE.84.041906 that show movies of the five different regimes (parachute, unconfined slipper, confined slipper, centered snaking, and off-centered snaking).
[22] H. Noguchi and G. Gompper, Proc. Natl. Acad. Sci. USA **102**, 14159 (2005).
[23] V. Vitkova, M. Mader, and T. Podgorski, Europhys. Lett. **68**, 398 (2004).
[24] G. Coupier, B. Kaoui, T. Podgosrki, and C. Misbah, Phys. Fluid **20**, 111702 (2009).
[25] T. Fischer, M. Stohr-Lissen, and H. Schmid-Schonbein, Science **202**, 894 (1978).
[26] S. Doddi and P. Bagchi, International Journal of Multiphase Flow **34**, 966 (2008).
[27] P. Bagchi and R. M. Kalluri, Phys. Rev. E **80**, 016307 (2009).
[28] T. Biben, A. Farutin, and C. Misbah, Phys. Rev. E **83**, 031921 (2011).
[29] A. Farutin and C. Misbah, Phys. Rev. E **84**, 011902 (2011).